Molecular Engineering Tuning of the Edge Environment of Atomic Nickel Active Sites for Efficient Alcohol Electrochemical-oxidation Reaction

Zhifu Liang[+], Daochuan Jiang[+], Xiang Wang, Mohsen Shakouri, Ting Zhang, Pengyi Tang, Jordi Llorca, Lijia Liu*, Marc Heggen, Rafal E. Dunin-Borkowski, Andreu Cabot*, Jordi Arbiol**

Z.F Liang, Ting Zhang, Prof. J. Arbiol

Catalan Institute of Nanoscience and Nanotechnology (ICN2),CSIC and BIST

Campus UAB, Bellaterra, 08193 Barcelona, Catalonia, Spain

Email: arbiol@icrea.cat

Dr. P. Y Tang

Shanghai Institute of Microsystem and Information Technology, Chinese Academy of Sciences, Shanghai 200050, China

Email: py.tang@mail.sim.ac.cn

Dr. Daochuan Jiang

School of Chemistry and Chemical Engineering, Anhui University, Heifei 230601, Anhui Province, China

Z.F Liang, X. Wang, Dr. J. J. Biendicho, Prof. J. R. Morante, Prof. A. Cabot

Catalonia Institute for Energy Research - IREC

Sant Adrià de Besòs, Barcelona, 08930, Catalonia, Spain

Email: acabot@irec.cat

Dr. Lijia Liu

Department of Chemistry, Western University, 1151 Richmond Street, London, ON

N6A5B7 Canada

Email: *lijia.liu@uwo.ca*

Dr. P. Y Tang, Dr. M Heggen, Prof. R E. Dunin-Borkowski

Ernst Ruska-Centre for Microscopy and Spectroscopy with Electrons and Peter Grünberg Institute Forschungszentrum Jülich GmbH 52425 Jülich, Germany

Dr. Mohsen Shakouri

Canadian Light Source, Saskatoon, S7N 0X4, Canada

Prof. J. Llorca
Institute of Energy Technologies, Department of Chemical Engineering and Barcelona Research Center in Multiscale Science and Engineering
Universitat Politècnica de Catalunya, EEBE, 08019 Barcelona, Catalonia Spain.

Prof. A. Cabot, Prof. J. Arbiol

ICREA

Pg. Lluís Companys 23, 08010 Barcelona, Catalonia, Spain

[+] These authors contributed equally to this work

* Corresponding authors

Abstract

Tuning the electronic structure of atomically dispersed actives sites through the modification of their edge coordination environment is an interesting strategy to design highly-efficient nickel based electrocatalysts as a promising alternative to noble metal materials for direct alcohol-based fuel cells. Herein, we report a new organic framework with atomically dispersed nickel. The addition of carbonyl (C=O) groups to the organic framework greatly enhances the electrocatalytic efficiency of the material for direct alcohol electro-oxidation (DAEO) in alkaline solution. The coordination structure and the presence of the carbonyl functional group was confirmed by X-ray absorption fine spectroscopy (XAFS) and Fourier Transform Infrared Spectroscopy (FTIR), respectively. Density functional theory (DFT) calculations reveal that the introduction of the carbonyl functional groups enhance the absorption for alcohol. The as-prepared nickel based organic framework and carbon nanotube composites (namely Ni-2D-O-SA-CNT) exhibits excellent catalytic activity and durability at the potential range mainly for methanol (106 mA cm^{-2} at 0.6 V vs Hg/HgO), ethanol (101 mA cm^{-2}) and benzyl alcohol (77 mA cm^{-2}). The remarked boosting electrocatalytic activity for DAEO can be attributed to the introduction the carbonyl group in the edge chemical environment to enhance the absorption for alcohol. Our work not only introduces a promising Ni-based atomically dispersed catalysts, but also demonstrates a new strategy for designing and tuning the chemical electronic structure for obtaining efficient catalysts for energy and electrochemical conversion reaction.

Keywords: molecule-based atomically dispersed nickel catalysts, edge environment tuning, organic framework, direct alcohol electro-oxidation reaction

Introduction

Direct alcohol fuel cells (DAFCs) are consider as one of promising energy generators due to their numerous advantages, such as a high theoretical energy density and energy conversion efficiency, an environmentally friendly composition, a simple operation, a low working temperature, the low cost of the produced methanol fuel and its easy production, transport and storage.[1] To promote the commercialization of alcohol fuel cells, the development of efficient catalysts for the anodic reaction of methanol oxidation is very critical. During the past years, platinum- and palladium-based noble metal catalysts were widely explored for DAFCs as they could work as efficient electrocatalysts for the alcohol electro-oxidation reaction, such as electrochemical oxidation for methanol and ethanol in DAFCs. [2-3] However, the high cost and limited source of noble metal-based catalysts and the carbon monooxide poisoning effect of platinum have been the main bottlenecks for restricting the commercial development of DAFCs. Therefore, searching for efficient and durable Pt-free electrocatalysts as substitutes for noble metals is one of the focus of current research interests in DAFCs.

In recent years, a variety of non-precious transition metal-based catalysts have achieved great progress as promising and suitable electrocatalysts for alcohol electro-oxidation.[4-5] Among them, nickel-based catalysts, because of its good surface oxidation properties, low price and abundant reserves, are considered by researchers to be one type of the best active catalysts candidates for alcohol electrochemical-oxidation because of its good surface oxidation properties, low price and abundant reserves. Many Ni-based species, such as $Ni_{0.75}Cu_{0.25}$,[6] NiSn alloy,[7] $Ni_{93}Bi_7$,[8] NiSe,[9] NiO,[10] Metal organic frameworks with $Ni(OH)_4$,[11] and Ni, Co hydroxide [12] have been tested as catalysts for alcohol electrochemical-oxidation. However, the electrochemical Alcohol Oxidation Reaction (AOR) onset potential, toxicity tolerance and stability of these catalysts are still not satisfying. Therefore, it is still necessary to develop novel strategies for designed efficient new nickel-based catalysts and with improved activity, lower or even non-toxicity and high stability, to

obtain novel non-precious metal based catalysts.

Recently, two-dimensional (2D) covalent organic frameworks (COF) and metal organic frameworks (MOF) with a highly tunable pore structure, high density of active sites and a precise regulation of their structure and functionality, have aroused the broad interest as electrocatalysts.[13] These 2D materials have been utilized in many different applications such as the oxygen evolution reaction,[14] the oxygen reduction reaction,[15] or the carbon dioxide electrochemical reduction.[16-17] However, they have rarely been applied to the alcohol electrochemical-oxidation reaction. It is still a great challenge to develop a novel molecular tuning engineering strategy in order to achieve high efficient electrocatalysts for alcohol electrochemical-oxidation by combining the properties of 2D organic frameworks with those offered by nickel.

Here, we report the synthesis of a new molecular atomically dispersed nickel atom based 2D organic framework with the introduction of abundant carbonyl (C=O) functional groups at the edge of the nickel ion coordination environment. In addition, we further determine its atomic structure and the correlation with its electrocatalytic activity toward the AOR. The carbonyl group and the nickel coordination structure were investigated by Fourier Transform Infrared Spectroscopy (FT-IR) and X-ray absorption fine spectroscopy, revealing that the nickel ions coordinate with two nitrogen and two oxygen atoms to form the salophen structure NiN_2O_2.[18] By combining the advantage of the adsorption ability of the carbonyl functional groups for alcohol and the unsaturated coordination number of nickel ions, the as-prepared Ni-2D-O-SA-CNT displays outstanding electrocatalytic activity and durability for alcohol electrochemical-oxidation reaction, including methanol, ethanol and benzyl alcohol. Our observations suggest that the introduction of the carbonyl groups may promote the absorption of alcohol to favor the kinetics of AOR. The present work, may not only inspires the further development of more efficient atomically dispersed nickel based catalysts for fuel oxidation reaction, but also benefit other research fields related to electrochemical-organic synthesis, energy conversion and storage.

Results and Discussions

As shown in **Figure 1a**, the nickel based two-dimensional organic framework (**Ni-2D-O-SA**) with carbonyl functional group was solvothermally synthesized through a Schiff based reaction between 2,5-hydroxyterephthalaldehyde (HBC) and tetramino-benzoquinone (TABQ) in N-methyl-2-pyrrolidone (NMP). The obtained dark-black solid indicated the formation of a conjugated polymer, which was washed by water and methanol, respectively, to remove the small mass impurities and then dried under vacuum. For comparison, a reference sample composed of nickel based 2D-organic frameworks (**Ni-2D-SA**) without the carbonyl chemical groups was prepared under the same reaction condition via using the 1,2,4,5-benzenetetraamine tetrahydrochloride (TAB) to replace the TABQ (**Figure S1**).[18]

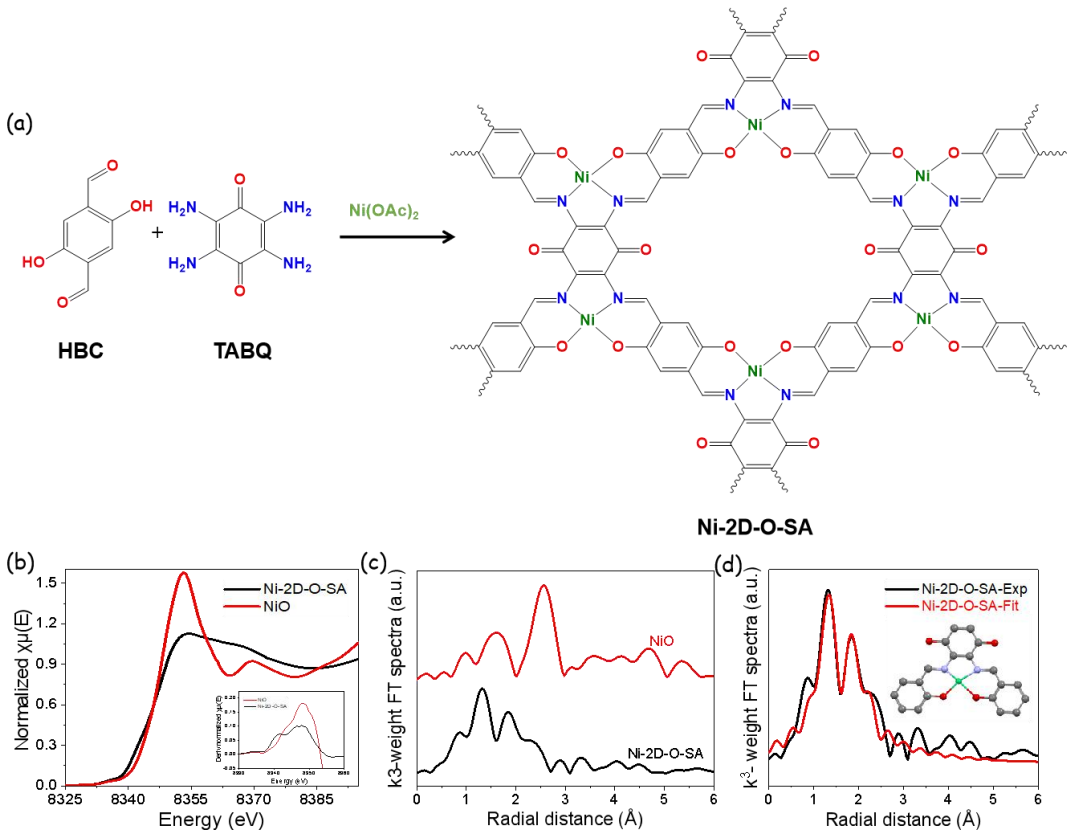

Figure 1 (a) Synthesis scheme of **Ni-2D-O-SA**, (b) the Ni K-edge XANES spectrum of **Ni-2D-O-SA** in comparison with the one of NiO (commercial powder), (c) the Fourier transformed Ni K-edge EXAFS spectra of **Ni-2D-O-SA** and NiO plotted in R-space, (d) Fourier transformed EXAFS spectra in R-space of Ni-2D-O-SA and the

fitted curve.

The powder X-ray diffraction (XRD) pattern (**Figure S3**) obtained on the **Ni-2D-O-SA** powder showed that its structure was crystalline and layered. The XRD pattern was similar to that of graphite, showing a diffraction peak at at 26.29° for the (001) facets, indicating π-π layered stacking.[19] However, the XRD pattern for the **Ni-2D-SA** powder indicated that had a low crystallinity. The latest indicates that the introduction of carbonyl groups would enhance the crystallinity of the nickel based 2D-organic framework used here. Fourier Transform Infrared Spectrometry (FT-IR) was used to evaluate the chemical structure of the samples (**Figure S4**). Based on the FT-IR spectra, the signal for C=N appeared at 1642 cm^{-1} (for **Ni-2D-SA**) and 1648 cm^{-1} (for **Ni-2D-O-SA**), respectively. In addition, the disappearance of the characteristic peaks corresponding to the N-H stretching vibration (3367-3197 cm^{-1}) confirmed the formation of Ni-salophen structure units.[18] The vibration of the carbonyl bond (C=O) in **Ni-2D-O-SA** negatively shifted below 1600 cm^{-1}, and overlapped with other vibrations. The vibration peak for the C-(C=O)-C bond which is characteristic in the TABQ shifted from 1140 cm^{-1} to 1010 cm^{-1} (for **Ni-2D-O-SA**) due to the coordination effect and the attraction between the layers, demonstrating the successful introduction of the carbonyl groups in the organic frameworks.[20] X-ray photoelectron spectroscopy (XPS) was applied to analyze the chemical information of these two samples (**Figure S5** and **Figure S6**). The survey spectra obtained revealed the appearance of C, N, Ni, O resonance signals in both samples. The high -resolution XPS peaks at 400 eV and 532 eV were assigned to N1s and Os respectively.[21] The high-resolution Ni2p spectrum showed two main peaks at 856 eV and 873.3 eV corresponding to Ni2p3/2 and Ni2p/1/2 respectively, together with their related satellite peaks.[22-23]

To further confirm the local environment near Ni of **Ni-2D-O-SA**, the X-ray absorption fine structure (XAFS) at the Ni K-edge was examined (**Figure 1b-d and Figure S7**). We first compare the spectral features of Ni-2D-O-SA with the one of NiO at the near-edge (i.e. X-ray absorption near-edge structure, XANES). As shown

in **Figure 1b**, the absorption onset of Ni-2D-O-SA occurs at an energy slightly lower than the one of NiO. The difference is more clearly to see when the two spectra are plotted in the first derivative (inset of Figure 2b). The main absorption peak of Ni-2D-O-SA also has a lower intensity. Both features indicate that compare to NiO where Ni is fully surrounded by O, Ni in Ni-2D-O-SA are surrounded by elements with less electronegativity (i.e. N substituting O).

A more quantitative picture can be obtained by analyzing the EXAFS features of the spectrum. Fourier transformed (FT) EXAFS is shown in **Figure 1c**, and the fitted (**Figure 1d**) curve suggests Ni is coordinated with two N atoms and two O atoms, at a bond length 1.87 Å and 2.05 Å, respectively. Contribution at longer radial distance comes from C atoms with coordination number of 6 and a bond length of 2.65 Å Detailed fitting parameters can be found in **Table S1**.

The XAFS analysis provides strong evidence of the formation of the NiN_2O_2 salophen structure unit in Ni-2D-O-SA frameworks.

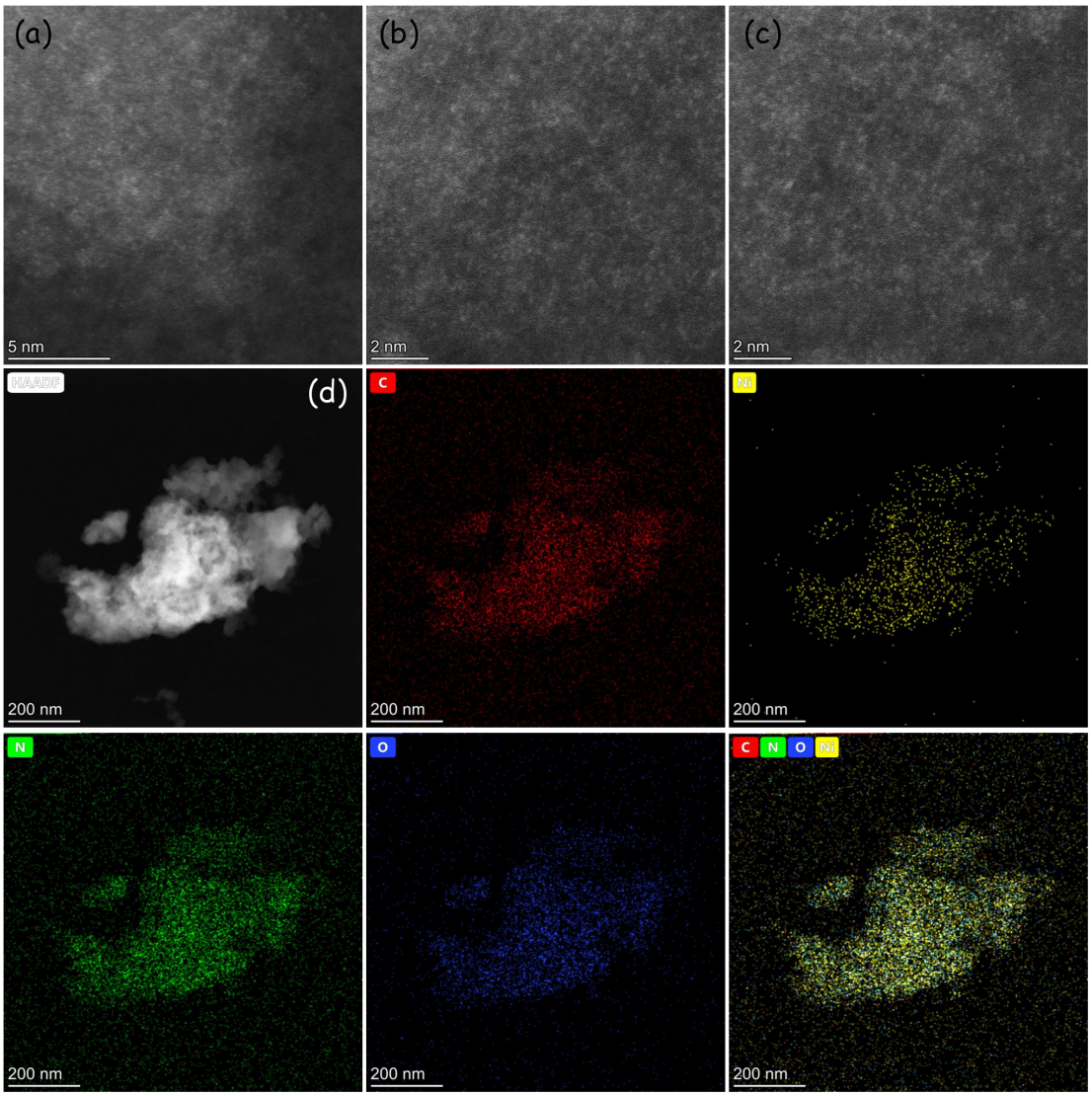

Figure 2. (a)-(c) HAADF-STEM images of Ni-2D-O-SA displaying the presence of atomically dispersed nickel atoms. (d) Low magnification HAADF-STEM image and EDS elemental mapping.

The scanning electron microscopy (SEM) images (**Figures S8a-b**) obtained show the cotton like morphology of the **Ni-2D-O-SA** sample. High angle annular dark field (HAADF)-aberration corrected (AC) scanning transmission electron microscopy (STEM) was used to analyse the dispersed state of the nickel atoms. As shown in **Figures 2a-c** and **Figure S9a-c**, high densities of isolated and homogeneously distributed nickel atoms were observed. The energy-dispersed X-ray spectroscopy (EDS) elemental mapping shown in **Figure 2d** and **Figure S9d** confirms that the Ni, C, N, O are uniformly distributed.

The N_2 adsorption-desorption isotherms at 77 K were conducted to evaluate the porosities of these two samples (**Figure S 10**). The Brunauer-Emmett-Teller surface areas of Ni-2D-SA and Ni-2D-O-SA are 21.1 and 83 m^2 g^{-1}, respectively, indicating that the introducing of the carbonyl functional group will degrease the surface area.

In order to improve the conductivity for these nickel-based organic frameworks and make them work as efficient electrocatalysts, multi-wall carbon nanotubes (CNT) were used as support to prepare composites (**Ni-2D-O-SA-CNT)** by physical mixing in dimethylformamide. The PXRD spectrum of these samples only showed a main peak at about 26° (**Figure S11**), which was assigned to the overlap between the CNT and the organic framework structures. The SEM images (**Figures S8c-d**) and STEM images (**Figure S12**) show the morphology of the **Ni-2D-O-SA-CNT** composite, which confirms a successful loading of the nickel-based organic frameworks in the CNTs.

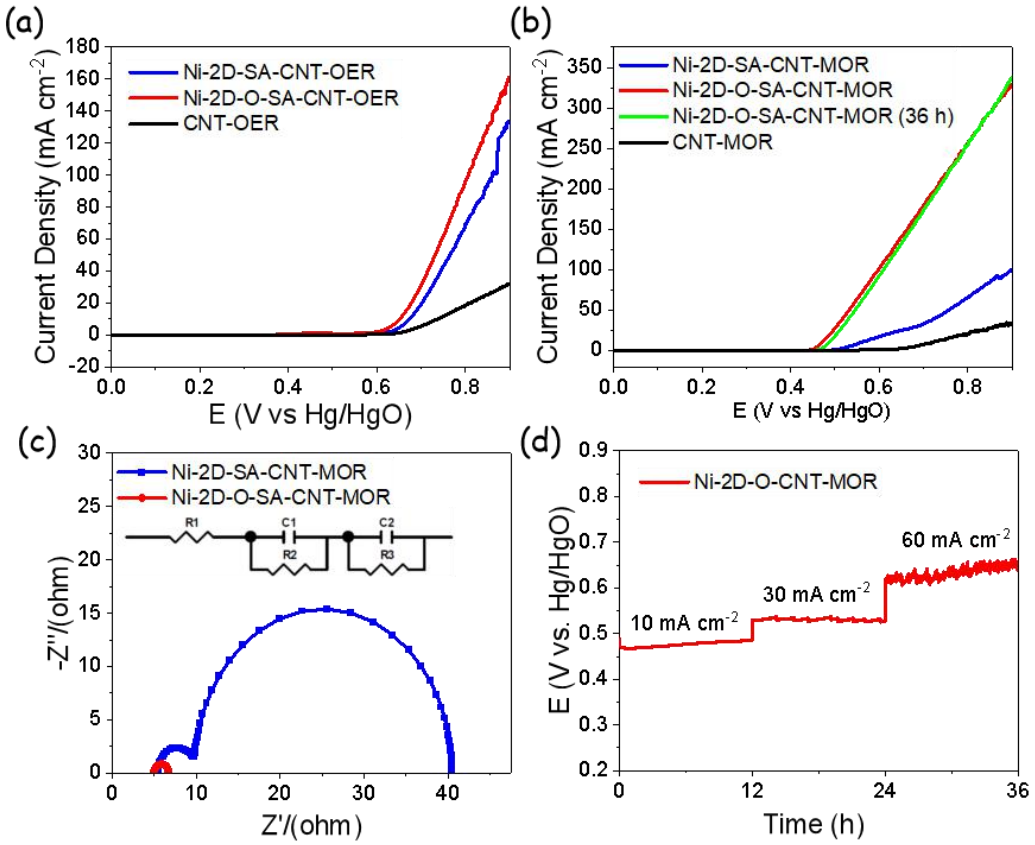

Figure 3. MOR with Linear sweep voltammetry (LSV) (without iR compensation) performance of **Ni-2D-SA-CNT**, **Ni-2D-O-SA-CNT** and reference carbon nanotubes

(CNTs) in (a) 1.0 M KOH; (b) 1 M KOH + 1 M Methanol from 0 to 0.9 V (versus Hg/HgO) at a scan rate of 5 mV s^{-1}. (c) The Nyquist plots of EIS for MOR at 0.56 V in 1 M KOH + 1 M methanol solution. (d) The long-term stability in CP curves of Ni-2D-O-SA-CNT at 10 mA cm^{-2}, 30 mA cm^{-2} and 60 mA cm^{-2}, respectively.

In order to investigate the performance of these as-prepared electrocatalysts, a three-electrode setup measurements were conducted in an electrolyzer; all curves were adopted without iR compensation. As shown in **Figures 3a** and **3b**, we tested the polarization curves of **Ni-2D-O-SA-CNT** and **Ni-2D-SA-CNT** by linear sweep voltammetry (LSV) in 1 M KOH and 1 M KOH +1 M methanol, respectively. The OER activity of **Ni-2D-O-SA-CNT** was scarcely improved compared to that of **Ni-2D-SA-CNT**. However, for methanol oxidation reaction (MOR), the **Ni-2D-O-SA-CNT** catalysts showed an excellent activity with current densities increasing from 31 mA cm^{-2} to 106 mA cm^{-2} at the range of 0.5 to 0.6 V versus Hg/HgO, which was about 6 times higher compared to that of **Ni-2D-SA-CNT**. According these results, it is demonstrated that the introduction of the carbonyl group (C=O) at the edge environment of the dispersed Ni-atoms active sites provides a much better catalytic activity for the methanol electrochemical-oxidation reaction (MOR). The charge transfer resistances of these two catalysts were evaluated to gain more knowledge on the electrode kinetics for OER and MOR. **Figure 3c** The Nyquist plots of Electrochemical Impedance Spectra (EIS) for **Ni-2D-O-SA-CNT** (Figure 3c) presents smaller semicircle diameter which corresponds the charge transfer resistance (R_3) than that for **Ni-2D-SA-CNT** at the potential of 0.56 V in 1 M KOH + 1 M Methanol electrolyte, indicating that the faster MOR kinetics of **Ni-2D-O-SA-CNT**. Again, this latest results indicates that sample **Ni-2D-O-SA-CNT** presents a highly efficient charge transport and favorable MOR kinetics at the 1 M KOH + 1 M Methanol electrolyte interface.[27] However, for the OER, the charge transfer resistance of **Ni-2D-O-SA-CNT** is very close to that of **Ni-2D-SA-CNT** at 0.67 V (**Figure S13b**), this is consistent with the OER performance for these two catalysts. As shown in the chronopotentiometry (CP) curve (**Figure 3c**), the **Ni-2D-O-SA-CNT**

electrocatalyst could keep current densities of 10 mA cm^{-2} for 12h with about 2.1% increase in the required potential, while there was only a 0.57% increase in the current densities of 30 mA cm^{-2} and about 4.8% increase in the current densities of 60 mA cm^{-2}, which should be attributed to the consumption of the methanol. After the chronopotentiometry tests, we also conducted the LSV test again with the used electrocatalysts in a fresh 1 M KOH + 1 M Methanol electrolyte (**Figure 3b**). The LSV curves of the catalyst after 36 h showed almost the same results as those obtained with the fresh electrocatalysts in the initial electrolyte, demonstrating the excellent stability of the **Ni-2D-O-SA-CNT** sample in the MOR process.

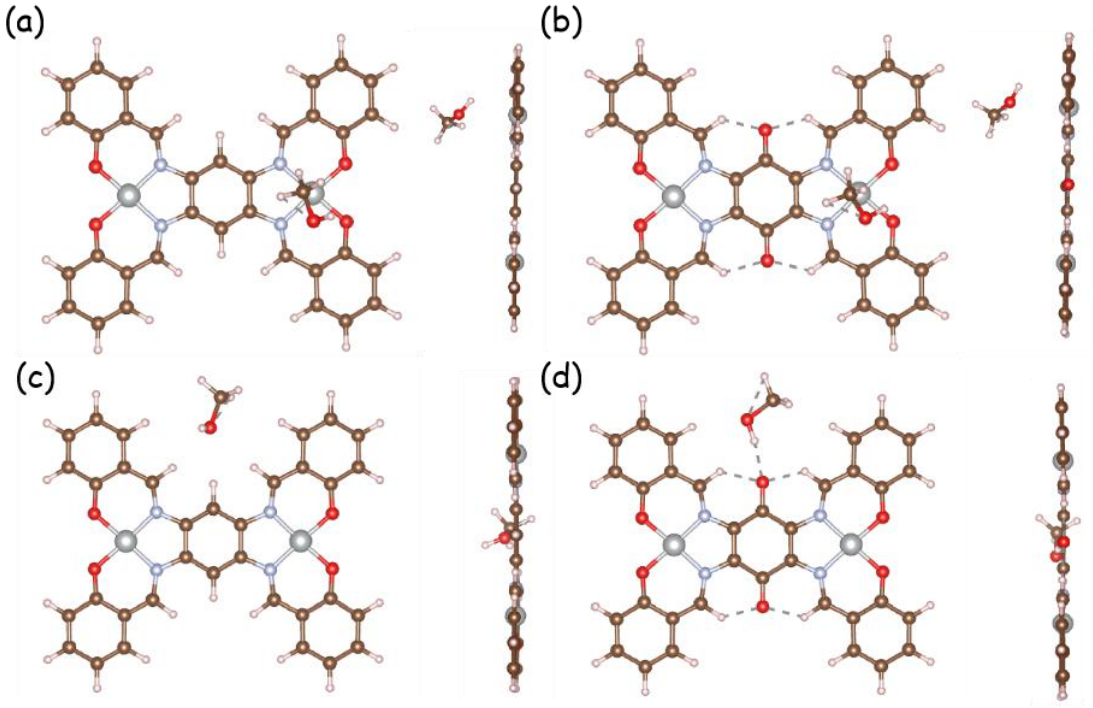

Figure 4. The optimal methanol adsorption configurations on the top position of Ni site in both **Ni-2D-SA (a)** and **Ni-2D-O-SA (b);** the optimal methanol adsorption configurations on the top position of carbonyl site in both **Ni-2D-SA (c)** and **Ni-2D-O-SA (d).**

Methanol adsorption is the initial step for MOR and the adsorption behavior is crucial for MOR activity. In order to understand the contributions of C=O group modification for the methanol adsorption, the density functional theory (DFT) calculations were carried out. **Figure 4** show the optimal methanol adsorption configurations on the top

position of Ni site in both **Ni-2D-O-SA** and **Ni-2D-SA**. The adsorption behaviors are evaluated based on the adsorption energies, H-O-CH_3 angle and the adsorption distance (d) between the O atom of methanol molecular and Ni atom in the monolayer 2D organic framework. The results show that the adsorption energy is -0.248 eV and -0.225 eV in **Ni-2D-SA** and **Ni-2D-O-SA**, respectively. The negative adsorption energies in both cases suggest that methanol adsorption is favored in thermodynamic. Interestingly, the adsorption distance in **Ni-2D-O-SA** is 3.11 Å, which is 5% shorter than that in **Ni-2D-SA**, indicating more effective adsorption of methanol molecule on the surface of **Ni-2D-O-SA**. What is more, the H-O-CH_3 angle in **Ni-2D-O-SA** increase to 109.04 ° from the original 108.25°. In sharp contrast, the H-O-CH_3 angle in **Ni-2D-SA** remain almost unchanged after optimized. Hence, **Ni-2D-O-SA** can facilitate the activation of methanol molecule. We also identify the O of C=O group as the adsorption site, it is observed that methanol molecule tends to adsorb at such O site in a configuration that OH group in the methanol is parallel to the surface. The shortest distance between the methanol molecule and the surface is 1.87 Å, which is much smaller than that case (2.5 Å) in Ni-2D-SA surface. Based on the DFT calculations, it is reasonable to conclude that the addition of carbonyl (C=O) groups to the organic framework can result in more effective adsorption as well as activation of methanol molecule. Therefore, **Ni-2D-O-SA** is more active for MOR catalysis than **Ni-2D-SA**.

To explore the universal applicability of the molecular designed strategy and the electrocatalytic activities of **Ni-2D-O-SA-CNT** for other alcohols, we also conducted electrochemical-oxidation reactions on ethanol and benzyl alcohol. Whether it is for the ethanol electrochemical-oxidation (EOR) (**Figure 5a**) or for the benzyl alcohol electrochemical-oxidation (BOR) (**Figure 5b**), the **Ni-2D-O-SA-CNT** presents a superior electrocatalytic performance compared to that of **Ni-2D-SA-CNT**. Especially for the BOR as shown in the **Figure 5b**, the current density at 0.6 V (versus HgO/Hg) is about 77 mA cm^{-2} which is 7.9 times higher than that 9.7 mA cm^{-2} of **Ni-2D-SA-CNT**.

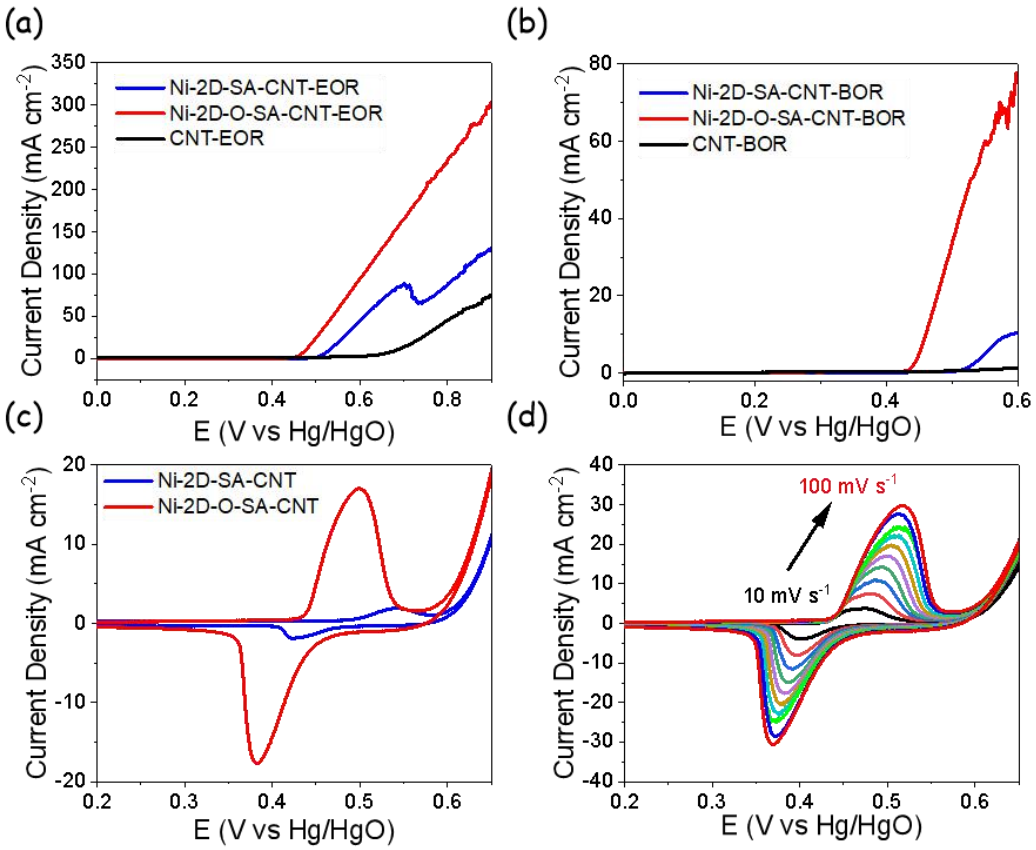

Figure 5. (a) EOR with Linear sweep voltammetry (LSV) performance of **Ni-2D-SA-CNT**, **Ni-2D-O-SA-CNT** and carbon nanotube (CNT) in 1 M KOH+1 M ethanol from 0 to 0.9 V (versus Hg/HgO) at a scan rate of 5 mV s^{-1}. (b) BOR with Linear sweep voltammetry (LSV) performance of **Ni-2D-SA-CNT**, **Ni-2D-O-SA-CNT** and the reference carbon nanotubes sample (CNTs) in 1 M KOH+0.1 M Benzyl alcohol from 0 to 0.9 V (versus Hg/HgO) at a scan rate of 5 mV s^{-1}. (c) Cyclic voltammograms of **Ni-2D-O-SA-CNT** and **Ni-2D-SA-CNT** electrocatalysts in 1 M KOH with the same potential sweep rate at 50 mV s^{-1}. (d) Cyclic voltammograms of Ni-2D-O-SA-CNT electrocatalysts in 1 M KOH with increasing potential sweep rate from 10 to 100 mV s^{-1} (gradient 10 mV s^{-1}).

Additionally, chronopotentiometry (CP) measurements were evaluated as stability tests on sample **Ni-2D-O-SA-CNT** for EOR. As shown in **Figure S15**, the **Ni-2D-SA-CNT** also exhibited a long-term stability for EOR, which is similar to that for MOR. The latest indicates that this sample could be favorable for the long term

application in fuel cells. For the BOR, the chronoamperometric (CA) measurement (**Figure S16**) shows that the current densities decay mainly due to the initial low concentration of benzyl alcohol and the consumption of the chemical conversion reaction. The EIS spectrum (**Figure S17**) for EOR and BOR are also similar to those shown for MOR, confirming that the **Ni-2D-O-SA-CNT** sample has also a highly efficient charge transport and is also highly favorable for EOR and BOR kinetics. XRD characterization was carried out on the catalysts after the electrocatalytic reaction in order to study the sample stability and possible evolution (**Figure S18**). Our results indicate that there is no presence of extra peaks in the XRD spectrum for Ni-2D-O-SA-CNT sample in comparison to the sample before the electrochemical tests, indicating that there is no formation of particles, segregation of other structures or phase transformation after the reactions, further confirming the stability of the as prepared **Ni-2D-O-SA-CNT** catalysts.

To further carry out the mechanistic study for the electrocatalytic activity in alkaline solution, **Figure 5c** exhibits the cyclic voltammograms (CV) of these two samples in the range from 0 V to 0.65 V in 1.0 M KOH electrolyte with a scan rate of 50 mV s^{-1}. The anodic peak of the **Ni-2D-O-SA-CNT** in the forward scan appears at 0.50 V vs Hg/HgO attributed to Ni^{2+} oxidation, and the cathodic peak in the backward appears at 0.38 V corresponding to the reduction of Ni^{3+} species. In the meanwhile, for the **Ni-2D-SA-CNT**, the anodic peak shifted to 0.54 V which is a more positive value, and the cathodic peak was placed at 0.42 V, which is less negative. The current density of the oxidation peak of Ni^{2+} in the **Ni-2D-O-SA-CNT** electrocatalyst was 19 mA cm^{-2} which is about 9.5 times higher than that of the **Ni-2D-SA-CNT** sample, showing just 2 mA cm^{-2}. These results indicate that the Ni^{2+} species in the **Ni-2D-O-SA-CNT** can get easily oxidized to Ni^{3+} and show a much faster electrochemical response. On the other hand, the ratio between the anodic and the cathodic peak current densities is close to 1, indicating that the Ni^{2+}/Ni^{3+} transformation reaction for these catalysts is reversible.[25] The surface coverage (Γ) of Ni^{2+}/Ni^{3+} in these two catalysts was also investigated.[26] The obtained Γ value for the

Ni-2D-O-SA-CNT sample was 1.32×10^{-7} mol cm^{-2}, which is two orders of magnitude higher than that for the **Ni-2D-SA-CNT** with 5.17×10^{-9} mol cm^{-2}, under the same conditions. **Figures 5d and S19b** display cyclic voltammograms of these two samples in 1.0 M KOH electrolyte with different scan rates ranging from 10 to 100 mV s^{-1}. The anodic and cathodic peak current densities could be fitted well with the square root of the voltage scan rate in the linear relationship, and both of them increased with the increasing of the scan rate (**Figure S19**), demonstrating that the electrochemical transformation reaction for Ni^{2+}/Ni^{3+} ascribed to diffusion control reaction.[25]

Conclusion

In conclusion, we synthesized a new nickel based two-dimensional organic framework successfully, and more importantly, we also proposed a facile strategy of molecular engineering to tune the edge coordination environments of nickel ion centers by introducing the carbonyl (C=O) groups to achieve an efficient alcohol electro-oxidation performance in alkaline solution. EXAFS and XANES analysis confirmed that the Ni salophen unit structure is NiN_2O_2 in the target organic frameworks. DFT calculations suggest that the introduction of the C=O functional groups favor the absorption of alcohol which results in a promotion of the electro-oxidation kinetics. The present work not only offers novel materials and a promising strategy to design more efficient nickel based atomically dispersed catalysts for alcohol fuel cells, but also for other fields, such as energy conversion and storage, electrocatalytic organic synthesis and so on.

Supporting Information

Supporting Information is available from online.

Acknowledgements

ICN2 is supported by the Severo Ochoa program from spanish MINECO (Grant No. SEV-2017-0706) and is funded by the CERCA Programme /Generalitat de Catalunya. Part of the present work has been performed in the framework of Universitat Autònoma de Barcelona Materials Science PhD program. Z. Liang acknowledges funding from MINECO SO-FPT PhD grant (SEV-2013-0295-17-1). This project has received funding from the European Union's Horizon 2020 research and inovation programme under grant agreement No 823717-ESTEEM3. The present work is supported by the European Regional Development Funds and by the Spanish MINECO through the projects SEHTOP, ENE2016-77798-C4-3-R, and ENE2017-85087-C3. X. Wang and T. Zhang thank the China Scholarship Council for the scholarship support. P. Tang acknowledge the Humboldt Research Fellowship. Authors acknowledge funding from Generalitat de Catalunya 2017SGR327 and 2017SGR1246. J. Llorca is a Serra Húnter Fellow and is grateful to MICINN/FEDER RTI2018-093996-B-C31, GC 2017 SGR 128 and to ICREA Academia program.

Conflict of interest

The authors declare no conflict of interest.

References

[1] E. Antolini, E. R. Gonzalez, *Journal of Power Sources* **2010**, *195*, 3431-3450.

[2] Y. Tong, X. Yan, J. Liang, S. X. Dou, *Small* **2021**, *17*, e1904126.

[3] M. A. F. Akhairi, S. K. Kamarudin, *International Journal of Hydrogen Energy* **2016**, *41*, 4214-4228.

[4] (a) S. Rezaee, S. Shahrokhian, *Applied Catalysis B: Environmental* **2019**, *244*, 802-813. (b) A. Badalyan, S. S. Stahl, *Nature* **2016**, 535, 406-410.

[5] G. M. K. Tolba, N. A. M. Barakat, A. M. Bastaweesy, E. A. Ashour, W. Abdelmoez, M. H. El-Newehy, S. S. Al-Deyab, H. Y. Kim, *Journal of Materials*

Science & Technology **2015**, *31*, 97-105.

[6] X. Cui, P. Xiao, J. Wang, M. Zhou, W. Guo, Y. Yang, Y. He, Z. Wang, Y. Yang, Y. Zhang, Z. Lin, *Angew Chem Int Ed Engl* **2017**, *56*, 4488-4493.

[7] J. Li, Z. Luo, Y. Zuo, J. Liu, T. Zhang, P. Tang, J. Arbiol, J. Llorca, A. Cabot, *Applied Catalysis B: Environmental* **2018**, *234*, 10-18.

[8] A. Dubale, Y. Zheng, H. Wang, R. Hübner, Y. Li, J. Yang, J. Zhang, N. Sethi, L. He, Z. Zheng, W. Liu, *Angew Chem Int Ed Engl* **2020**, *132*, 13995-14003.

[9] B. Zhao, J. Liu, C. Xu, R. Feng, P. Sui, L. Wang, J. Zhang, J. L. Luo, X. Z. Fu, *Advanced Functional Materials* **2020**, *31*.

[10] C. Liu, W. Zhou, J. Zhang, Z. Chen, S. Liu, Y. Zhang, J. Yang, L. Xu, W. Hu, Y. Chen, Y. Deng, *Advanced Energy Materials* **2020**, *10*.

[11] Y. Wu, J. Tian, S. Liu, B. Li, J. Zhao, L. Ma, D. Li ,Y. Lan, X. Bu, *Angew Chem Int Ed Engl* **2019**, *58*, 12185-112189.

[12] H. Huang, C. Yu, X. Han, H. Huang, Q. Wei, W. Guo, Z. Wang, J. Qiu, *Energy & Environmental Science* **2020**, *13*, 4990-4999.

[13] X. Zhao, P. Pachfule, A. Thomas, *Chem Soc Rev* **2021**, https://doi.org/10.1039/D0CS01569E.

[14] J. Du, F. Li, L.-C. Sun, *Chem Soc Rev* **2021**, 50, 2663-2695.

[15] S. Royuela, E. Martinez-Perinan, M. P. Arrieta, J. I. Martinez, M. M. Ramos, F. Zamora, E. Lorenzo, J. L. Segura, *Chem Commun (Camb)* **2020**, *56*, 1267-1270.

[16] H. Zhu, M. Lu, Y. Wang, S. Yao, M. Zhang, Y. Kan, J. Liu, Y. Chen, S. Liu, Y. Lan, *Nat Commun* **2020**, *11*, 497.

[17] J. Liu, D. Yang, Y. Zhou, G. Zhang, G. Xing, Y. Liu, Y. Ma, O. Terasaki, S. Yang, L. Chen, *Angew Chem Int Ed Engl* **2021**.

[18] T. Li, W.-D. Zhang, Y. Liu, Y. Li, C. Cheng, H. Zhu, X. Yan, Z. Li, Z.-G. Gu,

Journal of Materials Chemistry A **2019**, *7*, 19676-19681.

[19] B. P. Biswal, S. Chandra, S. Kandambeth, B. Lukose, T. Heine, R. Banerjee, *J Am Chem Soc* **2013**, *135*, 5328-5331.

[20] L. Wang, Y. Ni, X. Hou, L. Chen, F. Li, J. Chen, *Angew Chem Int Ed Engl* **2020**, *59*, 22126-22131.

[21] Y. Liao, H. Wang, M. Zhu, A. Thomas, *Adv Mater* **2018**, *30*, e1705710.

[22] F. L. Li, Q. Shao, X. Huang, J. P. Lang, *Angew Chem Int Ed Engl* **2018**, *57*, 1888-1892.

[23] J. Jin, Y. Zheng, S.-z. Huang, P.-p. Sun, N. Srikanth, L. B. Kong, Q. Yan, K. Zhou, *Journal of Materials Chemistry A* **2019**, *7*, 783-790.

[24] H. Yang, Q. Lin, C. Zhang, X. Yu, Z. Cheng, G. Li, Q. Hu, X. Ren, Q. Zhang, J. Liu, C. He, *Nat Commun* **2020**, *11*, 593.

[25] A. J. Bard, L. R. Faulkner, *Electrochemical Methods Fundamentals and applications* **2001**.

[26] D. Chen, S. D. Minteer, *Journal of Power Sources* **2015**, *284*, 27-37.

[27] Gao. Chen, Y. Luo, L. Ding, H. Wang, *ACS Catal.* **2018**, *8*, 526-530.